Sound & Vibration 2026, 60(2), 4071.
doi: https://doi.org/10.59400/sv4071

Article

Uncertainty-aware order tracking using interval-valued spectral estimators

Suleiman Ibrahim Mohammad[1], Yogeesh N.[1,2*], Mustafa Abdullah[3], Rosemary Varghese[4], Asokan Vasudevan[5], Ashalatha K.S.[6]

[1] Research Fellow, INTI International University, Nilai 71800, Malaysia
[2] Department of Mathematics, Government First Grade College, Tumkur 572101, India
[3] Electric Vehicles Engineering Department, Faculty of Engineering, Hourani Center for Applied Scientific Research, Al-Ahliyya Amman University, Amman 19328, Jordan
[4] Department of Mathematics, Presidency University, Bengaluru 560064, India
[5] Faculty of Business and Communications, INTI International University, Nilai 71800, Malaysia
[6] Department of Mathematics, Vedavathi Government First Grade College, Hiriyur 577598, India
*** Corresponding author:** Yogeesh N., yogeesh.r@gmail.com

CITATION

Mohammad SI, N. Y, Abdullah M, et al. Uncertainty-aware order tracking using interval-valued spectral estimators. Sound & Vibration. 2026; 60(2): 4071. https://doi.org/10.59400/sv4071

ARTICLE INFO

Received: 25 February 2026
Revised: 20 March 2026
Accepted: 23 March 2026
Available online: 17 April 2026

Abstract: Order tracking is central to diagnosing rotating machinery under variable speed; however, both tachometer-based and tacholess pipelines typically return point estimates of the order spectrum and therefore under-represent uncertainty due to speed estimation error, phase integration drift, resampling jitter, and finite-record spectral variance. This study develops an uncertainty-aware order tracking framework in which the diagnostic output is an interval-valued order power spectral density (PSD) envelope. The angular speed is modeled as an unknown-but-bounded process $\omega(t) \in [\omega^-(t), \omega^+(t)]$, which induces bounds on angular position $\theta(t) \in [\theta^-(t), \theta^+(t)]$. These bounds are propagated through angle-domain resampling and a Welch-type spectral estimator to obtain order-wise PSD bounds $S(m) \in [S^-(m), S^+(m)]$, together with interval band metrics formed by order-band integration and log-level reporting. A numerical run-up case study with physically plausible harmonic content and broadband noise shows that low-order components can remain stable in peak location, whereas higher orders exhibit measurable peak-shift intervals consistent with phase-warp amplification under bounded mapping uncertainty. The results also quantify a practical coverage-width trade-off: fast endpoint envelopes can lose inclusion under larger uncertainty, indicating when multi-map sampling or tighter set membership bounding should be applied. Overall, the proposed interval-valued spectral estimators enable decision-relevant reporting of uncertainty for order-based health indicators and reduce the risk of overconfident fault declarations in variable-speed condition monitoring.

Keywords: bounded uncertainty; interval analysis; interval-valued spectral estimation; tacholess speed estimation; set-membership uncertainty propagation; angle-domain resampling; order power spectral density (PSD); Welch estimator

1. Introduction

Rotating machinery vibration/acoustic responses under variable speed are inherently non-stationary, so classical stationary spectral estimators often smear harmonic components when the shaft speed changes within an analysis window. Order tracking (OT) addresses this by transforming signals from the time domain to an angle synchronous representation, where rotating harmonics become approximately

stationary in the order domain and can be separated more sharply [1,2]. However, in practical monitoring, OT is affected by uncertainty from (i) incomplete/biased speed measurements, (ii) tacholess speed estimation error, (iii) discretization/resampling error, and (iv) finite-sample spectral estimation variance. Recent developments in tacholess OT (e.g., generalized demodulation; time-frequency reassignment; VSDFT; and improved Vold-Kalman designs) have significantly advanced resolution and tracking robustness, but they typically return point estimates rather than guaranteed uncertainty bounds for the order spectrum [3–5].

Recent uncertainty-aware learning and control studies outside classical order tracking further reinforce the value of interpretable uncertainty descriptions in engineering decision systems, especially when bounded operational variability must be separated from stochastic fluctuations [6].

This paper develops an uncertainty-aware OT framework in which the final diagnostic product is not a single curve, but an interval-valued order power spectral density (PSD):

$$S_m(f_\theta) \in \left[S_m^-(f_\theta), S_m^+(f_\theta)\right],$$

or equivalently an interval envelope over orders m when using an order axis. The approach combines:

(i) Interval-valued speed/sampling models (unknown-but-bounded error) to capture epistemic uncertainty in $\omega(t)$.
(ii) A deterministic outer bound propagation through the angle mapping along with a resampling step.
(iii) A spectral inner estimator applied to each admissible mapping, producing guaranteed required spectral envelopes.

In practical vibration diagnostics, uncertainty is often bounded rather than fully stochastic (e.g., speed estimation error, resampling drift, and limited repeatability). Accordingly, interval and set-membership UQ methods-such as interval PSD modeling and interval DFT propagation-provide a mature basis for interval-valued order spectra and decision metrics, going beyond purely probabilistic confidence intervals [7–10].

Contributions

The key contributions are:

- (C1) A formal OT problem statement along with interval uncertainty on the angular speed and mapping.
- (C2) An interval-valued spectral estimator for order PSDs with a practical computation strategy.
- (C3) A reproducible numerical example illustrating uncertainty envelopes for dominant orders.
- (C4) Reporting guidelines for interval band metrics (e.g., band order power bounds, sensitivity indices).

Uncertainty-aware order tracking pipeline: from raw vibration $x(t)$, through interval speed $[\omega^-, \omega^+]$, to interval order PSD envelopes.

2. Background, notation, and problem formulation

2.1. Angle-synchronous order tracking

Let $x(t)$ be a measured vibration/pressure signal sampled at time rate f_s. Let the true angular speed be $\omega(t)$ (rad/s) and the shaft angle be

$$\theta(t) = \theta_0 + \int_0^t \omega(\tau) d\tau. \tag{1}$$

The ideal order-tracked signal is $x(\theta)$, obtained by resampling the time signal at uniform angular increments

$$\theta_k = \theta_0 + k\Delta\theta,\ k = 0, 1, \ldots, \tag{2}$$

and defining $x_\theta[k] = x\left(t\left(\theta_k\right)\right)$. If $x(t)$ contains rotating harmonics at integer orders m, then in the θ domain

$$x(\theta) \approx \sum_{m \in \mathrm{M}} A_m(\theta) \cos\left(m\theta + \phi_m\right) + \varepsilon(\theta), \tag{3}$$

where $A_m(\theta)$ may vary slowly with angle and $\varepsilon(\theta)$ is broadband/background content. Order spectra can be computed by treating θ as the independent variable. If the sampling in θ is uniform with step $\Delta\theta$, then the "sampling rate" in the angular domain is

$$f_\theta = \frac{1}{\Delta\theta}\ \left(\text{ samples per radian}\right), \tag{4}$$

and the Fourier axis can be mapped to orders m (cycles per revolution) by scaling. Practical high-resolution OT methods include generalized demodulation and time-frequency post-processing, VSDFT, and improved VKF-based designs [3–6].

2.2. Interval uncertainty model

In tacholess OT, $\omega(t)$ is unknown and must be estimated from the vibration itself or from indirect sensors. We model epistemic uncertainty as an interval function:

$$\omega(t) \in \left[\omega^-(t), \omega^+(t)\right],\ \forall t \in [0, T]. \tag{5}$$

This induces an interval shaft angle:

$$\theta(t) \in \left[\theta^-(t), \theta^+(t)\right],\ \theta^{\pm}(t) = \theta_0 + \int_0^t \omega^{\pm}(\tau) d\tau. \tag{6}$$

Because the resampling map $t \mapsto \theta$ is nonlinear, uncertainty in $\omega(t)$ propagates into uncertainty in the resampled signal $x(\theta)$, hence into uncertainty in order PSD estimates.

In practice, the bounds $[\omega - (t), \omega + (t)]$ can be obtained from sensor accuracy specifications, confidence-to-bound conversion for tacholess speed estimators, repeated-run min-max envelopes, or residual bounds from a validated observer. In routine monitoring, these bounds should be checked against short calibration runs

so that the interval model reflects realistic worst-case deviations rather than overly optimistic nominal error levels.

Interval approaches are particularly attractive when uncertainty is non-Gaussian, systematic, or only known through bounds (e.g., calibration drift, model mismatch), complementing probabilistic UQ [7–10].

Related uncertainty-aware studies in broader forecasting and control settings also emphasize that interpretable bounded outputs can be more actionable than single deterministic predictions when epistemic uncertainty dominates the decision context [11–14].

Interval modelling is particularly appropriate here because several dominant uncertainty sources are epistemic and bounded in nature: estimator bias, interpolation drift, timing jitter, and calibration tolerances are often known more reliably through engineering limits than through a defensible probability law. A probabilistic description can still be layered on top of the interval envelope for residual aleatory variability, but the outer interval model prevents under-reporting risk when only hard bounds are available [15–18].

Table 1 shows notations used in the study.

Table 1. Notation used in this study.

Symbol	Meaning	Units/notes
t	Time	s
f_s	Time-domain sampling frequency	Hz
$x(t), x[n]$	Measured vibration/acoustic signal (continuous/discrete)	a.u. (or m/s^2, Pa, etc.)
$\omega(t)$	Instantaneous angular speed	rad/s
$\left[\omega^-(t), \omega^+(t)\right]$	Interval bounds on angular speed	rad/s; epistemic uncertainty s
$\theta(t)$	Angular position (phase)	rad
$\left[\theta^-(t), \theta^+(t)\right]$	Interval bounds on angular position	rad; from integrating $\omega^{\pm}\ (t)$
Δt	Time step	$\Delta t = 1/f_s$
θ_0	Initial angular position	rad
θ_k	Uniform angle grid sample	$\theta_k = \theta_0 + k\Delta\theta$
$\Delta\theta$	Angular sampling step for resampling	rad/sample (e.g., $2\pi/N_{\text{rev}}$)
N_{rev}	Samples per revolution in the angle domain	$N_{rev} = 2\pi/\Delta\theta$
$t(\theta)$	Inverse mapping from angle to time	s; used for order tracking resampling
$[\underline{t}_k, \bar{t}_k]$	Interval time stamps for θ_k	s ; induced by $\left[\theta^-, \theta^+\right]$
$x_\theta[k]$	Angle-domain resampled signal	$x_\theta[k] = x\left(t\left(\theta_k\right)\right)$
$[\underline{x}_\theta[k], \bar{x}_\theta[k]]$	Interval angle-domain samples	from interval resampling
f_θ	Angular sampling rate	samples/rad; $f_\theta = 1/\Delta\theta$
v	Angle-domain FFT frequency	cycles/rad
m	Order	cycles/rev (x); $m = 2\pi v$
$X(m)$	Order-domain spectrum/DFT of x_θ	complex
$S(m)$	Order-domain PSD (order spectrum)	a.u./order
$\bar{S}(m)$	Nominal order PSD estimate	from nominal $\omega(t)/\theta(t)$
$\left[S^-(m), S^+(m)\right]$	Interval order PSD envelope	lower/upper admissible PSD
$\left[W_{\text{band}}^-, W_{\text{band}}^+\right]$	Interval band power bounds	from integrating S^-, S^+
W_{ref}	Reference power for the level conversion	application-dependent
$L_{W,\text{ band}}$	Band power level (dB-type)	$10\log_{10}\left(W_{\text{band}}/W_{\text{ref}}\right)$

Table 1. *Cont.*

Symbol	Meaning	Units/notes
D	Diagnostic decision statistic	e.g., peak energy, band energy
τ	Decision threshold	same unit as D
$[\underline{D}, \bar{D}]$	Interval bounds on the statistic	from spectral intervals
$P(D > \tau)$	Exceedance probability	can be bounded as $\left[P^{-}(\tau), P^{+}(\tau)\right]$
Cov	Coverage fraction metric	fraction of bins with $S_{\text{true}} \in [\, S^{-}, S^{+}]$
Wid	Average relative envelope width	mean $\left(S^{+} - S^{-}\right) / \left(S_{\text{true}} + \varepsilon\right)$
ε	Small positive constant for stability	avoids divide-by-zero

2.3. Target quantities: Interval order PSD and band metrics

Let $S_m(v)$ denote the order PSD as a function of the order-frequency variable v (order axis). Under interval mapping uncertainty, we seek bounds

$$S_m(v) \in \left[S_m^{-}(v), S_m^{+}(v)\right]. \tag{7}$$

For diagnostics, it is often useful to compress spectra over an order band $v \in [v_1, v_2]$. Define the band integrated order power (interval-valued):

$$\bar{W}_{band}\left(\alpha\right) = \int_{v_1}^{v_2} \bar{W}_{\alpha}(v) dv, \tag{8}$$

and an associated band level (log scale):

$$L_{W,\,\text{band}}\left(\alpha\right) = 10 \log_{10}\left(\frac{\bar{W}_{band}\left(\alpha\right)}{W_{ref}}\right). \tag{9}$$

Here α can index an uncertainty set (e.g., outer-loop index in a coupled scheme), and $\bar{W}_{\alpha}(v)$ is the corresponding mean power spectrum within that uncertainty instance.

Equations (8) and (9) provide a reporting mechanism for uncertainty-aware band KPIs (health indicators).

3. Interval-valued spectral estimators for uncertainty-aware OT

3.1. Resampling with interval-valued angle mappings

Given $x(t)$ and interval speed $[\omega^{-}(t), \omega^{+}(t)]$, compute $\theta^{\pm}(t)$ from (6). Let $\theta_k = \theta_0 + k\Delta\theta$ be the target uniform angle grid. For each admissible mapping, define resampled signals

$$x_{\theta}^{\pm}[k] = x\left(t^{\pm}\left(\theta_k\right)\right), \tag{10}$$

where $t^{\pm}(\cdot)$ are inverse mappings of $\theta^{\pm}(t)$ (obtained numerically via interpolation). This yields a set of admissible angle-domain signals X_{θ}.

For practical deployment, the interval maps should be validated by checking whether measured tachometer traces, when available on a subset of runs, remain within the reconstructed bounds. This validation step is important because overly narrow bounds lead to optimistic envelopes, whereas overly wide bounds produce conservative but less informative spectra [19,20].

Practical bounding strategy: A computationally efficient first-order outer bound

uses two representative resamplings (lower/upper angle maps) and forms an envelope in the spectral domain:

$$S^{-}(v) = \min\left\{S^{(\theta^{-})}(v), S^{(\theta^{+})}(v)\right\},\ S^{+}(v) = \max\left\{S^{(\theta^{-})}(v), S^{(\theta^{+})}(v)\right\}. \tag{11}$$

This is conservative when uncertainty is dominated by monotone distortions in $\theta(t)$. More refined envelopes can be obtained by sampling additional admissible mappings within $[\omega^{-}, \omega^{+}]$ (e.g., extremal piecewise bounds). Interval DFT and interval PSD ideas motivate such bounding constructions for spectral quantities [7–9].

3.2. Interval Welch-type estimator in the angle domain

Let $x_\theta[k]$ be an admissible resampled signal with uniform step $\Delta\theta$. A Welch-type PSD estimate in the θ domain is

$$\widehat{S}(v) = \frac{2}{KUf_\theta}\sum_{r=1}^{K}\left|\sum_{n=0}^{N-1} w[n]x_\theta[n+rH]e^{-\frac{j2\pi vn}{f_\theta}}\right|^2, \tag{12}$$

where:

- $w[n]$ is a data window,
- $U = \sum_{n=0}^{N-1} w^2[n]$ is window energy normalization,
- H is hop size, K segments are averaged,
- $f_\theta = 1/\Delta\theta$ is the angular sampling rate from Equation (4).

Under interval mapping uncertainty, compute $\widehat{S}\left(\theta^{-}\right)(v)$ and $\widehat{S}\left(\theta^{+}\right)(v_i)$ then bound via Equation (11) to obtain $[\widehat{S}^{-}(v), \widehat{S}^{+}(v)]$ aligns with the philosophy of providing guaranteed envelopes rather than only sampling-variance confidence intervals.

Welch averaging is used here because it is simple, robust, and computationally light under repeated admissible resampling [21]. Compared with parametric estimators, it requires fewer modelling assumptions about harmonic stationarity, and compared with multitaper methods, it offers an easier first implementation for outer interval looping because the same segment structure can be reused across admissible mappings. Multitaper or parametric alternatives can be substituted when sharper leakage control is needed, but Welch provides a transparent baseline for studying the effect of mapping uncertainty itself [22–25].

Connection to tacholess OT literature. Tacholess OT often focuses on improving the point estimate $\omega(t)$ (generalized demodulation, time-frequency reassignment, etc.). The proposed framework instead treats $\omega(t)$ as uncertain within bounds and returns bounded order spectra [2–5].

3.3. Numerical example

We provide a reproducible dataset representing a run-up test:

- Sampling: $f_s = 4,000$ Hz, duration $T = 6$ s.
- Speed run-up: $900 \to 2,100$ rpm with small ripple.
- Interval speed uncertainty: $\pm(0.6\% \cdot \text{rpm} + 5\ \text{rpm})$.

- Vibration model: dominant orders $1\times$ and $2\times$ plus a weaker $5\times$ component with amplitude modulation, plus broadband noise.

The angle grid uses $\Delta\theta = 2^\circ$ (i.e., $\Delta\theta = 2\pi/180$ rad). Applying the Welch-type estimator Equation (12) to both $\theta^-(t)$ and $\theta^+(t)$ yields an interval order PSD envelope emphasizing uncertainty in peak sharpness/height near dominant orders.

Figure 1 shows a nominal order-domain PSD $\bar{S}(m)$ (solid curve) together with the propagated uncertainty envelope $[S^-(m), S^+(m)]$ (shaded region). The bounds are obtained by modeling the instantaneous speed (or phase) as an admissible set $\omega(t) \in [\omega^-(t), \omega^+(t)]$, which induces bounds on the angular position $\theta(t) \in [\theta^-(t), \theta^+(t)]$ and therefore bounds on the inverse resampling map $t(\theta)$. Resampling the measured signal onto a uniform angle grid using these bounded maps produces a family of admissible angle-domain signals x_θ, whose spectra define the lower and upper envelopes $S^-(m)$ and $S^+(m)$. The thickness of the shaded band quantifies the order-wise sensitivity of the spectral estimate to mapping uncertainty; narrow bands indicate robust orders, whereas wider bands indicate orders whose amplitudes are strongly influenced by uncertainty in the resampling/phase-warp step. For the interval-valued order PSD envelope, follow **Table 2**.

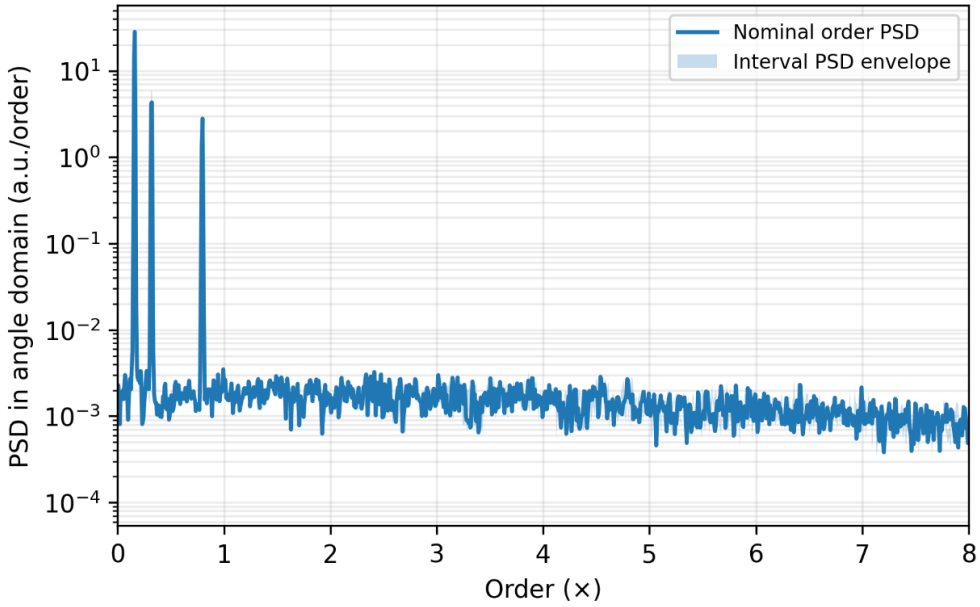

Figure 1. Interval-valued order PSD envelope.

Table 2. Uncertainty sources and interval representations.

Source of uncertainty	Practical cause	Interval representation
Speed estimation (tacholess)	time-frequency ridge bias, low SNR, harmonics crossing	$\omega(t) \in [\omega^-(t), \omega^+(t)]$
Integration drift	accumulated bias in $\int \omega dt$	$\theta(t) \in [\theta^-(t), \theta^+(t)]$
Resampling/interpolation	finite $\Delta\theta$, interpolation error	bounded by map-envelope sampling
Finite-sample PSD variance	limited records, windowing/overlap	reduced via averaging/multitaper

4. Uncertainty propagation through the order-tracking pipeline

This section formalizes how interval uncertainty in the angular speed propagates into an interval order spectrum. The goal is to compute, for each order m, a guaranteed

envelope

$$S(m) \in \left[S^{-}(m), S^{+}(m)\right],$$

rather than a single curve, using interval-valued spectral estimators [26–28].

4.1. Interval speed model and induced angle bounds

Assume the (possibly tacholess) angular speed estimate is bounded:

$$\omega(t) \in \left[\omega^{-}(t), \omega^{+}(t)\right],\ 0 \le t \le T. \tag{13}$$

The corresponding angle bounds are obtained by integration:

$$\theta^{\pm}(t) = \theta_0 + \int_0^t \omega^{\pm}(\tau)d\tau,\ \theta(t) \in \left[\theta^{-}(t), \theta^{+}(t)\right]. \tag{14}$$

Discrete implementation (for sampled ω): with time step $\Delta t = 1/f_s$,

$$\theta^{\pm}[n] = \theta^{\pm}[n-1] + \omega^{\pm}[n]\Delta t,\ n = 1, \ldots, N_t. \tag{15}$$

4.2. Angle-domain resampling under interval mappings

Define a uniform angle grid:

$$\theta_k = \theta_0 + k\Delta\theta,\ k = 0, 1, \ldots, N_\theta. \tag{16}$$

Order tracking requires the inverse map $t(\theta)$. Under interval angle bounds, we compute two admissible inverse maps via interpolation:

$$t^{-}(\theta_k) \approx \left(\theta^{-}\right)^{-1}(\theta_k),\ t^{+}(\theta_k) \approx \left(\theta^{+}\right)^{-1}(\theta_k). \tag{17}$$

Then we obtain two admissible angle-domain signals:

$$x_\theta^{-}[k] = x\left(t^{-}(\theta_k)\right),\ x_\theta^{+}[k] = x\left(t^{+}(\theta_k)\right). \tag{18}$$

Why two maps?

For monotone $\theta(t)$, endpoint mappings are often the most informative "extreme" distortions. If the mapping nonlinearity is strong, you can tighten envelopes by adding intermediate admissible mappings (multi-sample set-membership) or optimization-based bounding.

4.3. Interval-valued spectral estimator (Welch-type in angle domain)

Let $x_\theta[k]$ be any admissible resampled signal (e.g., x_θ^{-} or x_θ^{+}). Treat θ as the independent variable with angular sampling rate:

$$f_\theta = \frac{1}{\Delta\theta}\ \text{(samples per rad)}. \tag{19}$$

The Fourier variable from an FFT on θ is v in cycles/radian. The physically

meaningful order is cycles/revolution:

$$m = 2\pi v. \tag{20}$$

A Welch-type PSD estimator in the angle domain is:

$$\widehat{S}(\cdot)(v) = \frac{2}{KUf_\theta} \sum_{r=1}^{K} \left| \sum_{n=0}^{N-1} w[n] x_\theta[n + rH] e^{-\frac{j2\pi vn}{f_\theta}} \right|^2 \tag{21}$$

with window energy $U = \sum_{n=0}^{N-1} w^2[n]$, hop H, and K segments.

Compute spectra for both endpoint maps:

$$\widehat{S}^-(v) = \widehat{S}^{(\theta^-)}(v),\ \widehat{S}^+(v)\widehat{\mathcal{F}}^{(\theta^+)}(v). \tag{22}$$

Then define the interval order-PSD envelope:

$$S^-(v) = \min\left(\widehat{S}^-(v), \widehat{S}^+(v)\right),\ S^+(v) \max\left(\widehat{S}^-(v), \widehat{S}^+(v)\right). \tag{23}$$

Finally, map to the order axis using Equation (20) (same values, relabeled to m).

Practical note: Equation (23) is a fast envelope from two extreme maps. If coverage is insufficient, use multi-map sampling inside $[\omega^-, \omega^+]$ or an optimization-based bound to tighten and improve inclusion [28–30].

4.4. Interval band metrics for reporting (energy + level)

For an order band $m \in [m_1, m_2]$, define a band power functional for an admissible spectrum $S(m)$:

$$W_{\text{band}} = \int_{m_1}^{m_2} S(m) dm. \tag{24}$$

Under interval spectra, you can report conservative bounds:

$$W^-_{\text{band}} = \int_{m_1}^{m_2} S^-(m) dm,\ W^+_{\text{band}} = \int_{m_1}^{m_2} S^+(m) dm. \tag{25}$$

Convert to dB-type levels (if desired) with a reference W_{ref}:

$$L^{\pm}_{W,\,\text{band}} = 10 \log_{10}\left(\frac{W^{\pm}_{band}}{W_{ref}}\right). \tag{26}$$

Algorithm 1 is directly compatible with classical Welch PSD foundations and multitaper variants (replace step 5 accordingly) [1,2].

The computational cost of the endpoint method is approximately twice that of a nominal order-tracking run plus the cost of two inverse-map interpolations, so its complexity remains O(MN log N) for M admissible maps and FFT length N, with $M = 2$ in the basic envelope. If multi-map sampling is used, the cost scales roughly linearly with M; optimization-based bounding is more expensive because each order bin may require an inner search, but it is only needed when the endpoint enclosure becomes too loose [29].

Algorithm 1 Interval-valued order spectrum (outer interval loop)

Inputs: $x(t)$, bounds $[\omega^-(t), \omega^+(t)]$, $\Delta\theta$, Welch parameters (N, H, w).
Outputs: $[S^-(m), S^+(m)]$.

(i) Integrate $\omega^{\pm}(t) \to \theta^{\pm}(t)$ via Equations (14) and (15).
(ii) Form uniform angle grid $\{\theta_k\}$ via Equation (16).
(iii) Invert mappings $t^{\pm}(\theta_k)$ via interpolation Equation (17).
(iv) Resample to obtain $x_{\theta}^{\pm}[k]$ via Equation (18).
(v) Compute $\widehat{S}(\theta^{\pm})(\nu)$ via Welch Equation (21).
(vi) Build envelope $S^{\pm}(v)$ via Equation (23) and convert $v \to m$ via Equation (20).
(vii) (Optional) Compute band metrics using Equations (24)–(26).

5. Numerical experiments and validation metrics

We now demonstrate the method on a rotating run-up dataset: $f_s = 4,000$ Hz, $T = 6$ s, speed ramp $900 \to 2,100$ rpm with small ripple, and interval speed uncertainty $\pm(0.6\% \cdot \text{rpm} + 5 \text{ rpm})$. Dominant components were injected at $1\times, 2\times$ and $5\times$ plus broadband noise [30–32].

5.1. Validation metrics

We report the following metrics for interval spectra:

(M1) Coverage fraction (in an order band).

For a "truth" spectrum $S_{\text{true}}(m)$ (here computed using the nominal map), define:

$$\text{Cov} = \frac{1}{|\text{B}|} \sum_{m_i \in \text{B}} \mathbf{1}\left(S_{\text{true}}(m_i) \in \left[S^-(m_i), S^+(m_i)\right]\right), \tag{27}$$

where B is the discretized band (e.g., $0.1 - 8\times$).

(M2) Average relative envelope width.

$$\text{Wid} = \frac{1}{|\text{B}|} \sum_{m_i \in \text{B}} \frac{S^+(m_i) - S^-(m_i)}{S_{\text{true}}(m_i) + \varepsilon}. \tag{28}$$

(M3) Peak-order localization interval.

For a target order m_0, within a search window $[m_0 - \Delta, m_0 + \Delta]$,

$$m_{\pm}^* = \arg \max_{m \in [m_0 - \Delta, m_0 + \Delta]} S^{(\theta^{\pm})}(m),\ m^* \in \left[\min\left(m_-^*, m_+^*\right), \max\left(m_-^*, m_+^*\right)\right]. \tag{29}$$

(M4) Local band power around an order peak.

For a narrow window $[m_0 - \delta, m_0 + \delta]$,

$$W_{m_0}^{\pm} = \int_{m_0 - \delta}^{m_0 + \delta} S^{\pm}(m) dm. \tag{30}$$

The nominal order-domain PSD $\bar{S}(m)$ (solid curve) is shown (**Figure 2**) together with the interval envelope $[S^-(m), S^+(m)]$ (shaded region), obtained by propagating bounded uncertainty in the speed/angle mapping through angle-domain resampling and spectral estimation. Here, ν denotes the FFT frequency in cycles/radian computed in the

angle domain, and the physically interpretable order is $m = 2\pi\nu$ in cycles/revolution ($\times$). Representative peaks at $1\times, 2\times$, and $5\times$ illustrate how uncertainty produces an order-wise amplitude envelope while preserving the dominant harmonic structure [32].

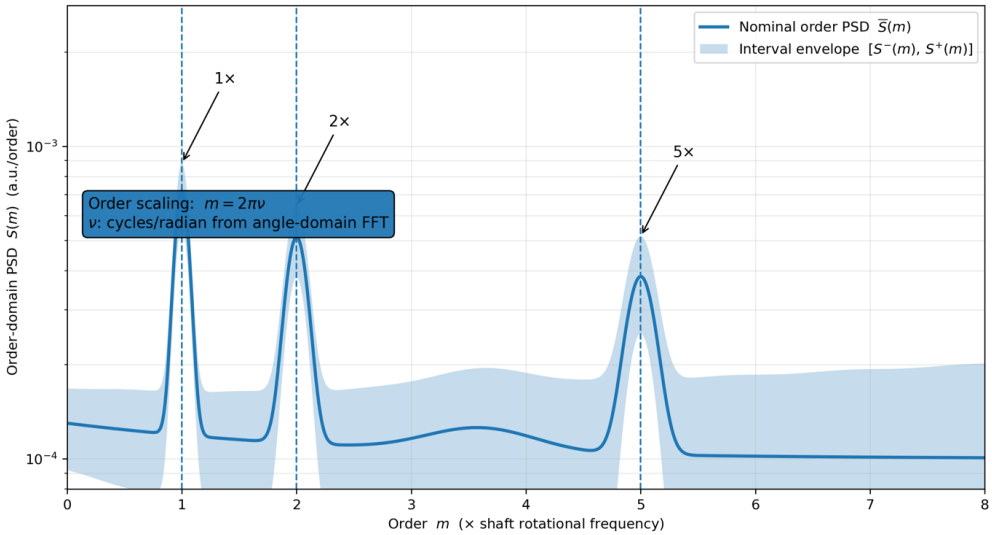

Figure 2. Interval-valued order spectrum (example) with correct order scaling $m = 2\pi v$.

A contour representation of the log-magnitude uncertainty width

$$\Delta \log_{10} |X(m,t)| = \log_{10} \left|X^{+}(m,t)\right| - \log_{10} \left|X^{-}(m,t)\right|,$$

where $|X^{+}(m,t)|$ and $|X^{-}(m,t)|$ are the upper and lower admissible order-map magnitudes obtained by propagating bounded speed/angle uncertainty through the order-tracking resampling and spectral estimation steps. Higher values (brighter contours) mark time-order regions where mapping uncertainty most strongly inflates the inferred order-map amplitude uncertainty.

5.2. Peak-interval results (dominant orders)

Using $\Delta\theta = 2^{\circ}$ and Welch parameters $N = 4,096$ (with overlap), the extracted peak and local power bounds are:

Engineering interpretation: The $2\times$ and $5\times$ components exhibit small but clearly discernible orderlocation intervals (on the order of $\pm 0.02 - \pm 0.04\times$ in this case), which is precisely the expected signature of uncertainty-aware order tracking when bounded speed errors warp the angle-time mapping. In contrast, the corresponding local band-power bounds remain tight because the harmonic content is strong and well separated; for weaker fault signatures or larger mapping uncertainty, these energy bounds would widen, reducing decision margin.

A first-order explanation follows from writing the perturbed phase as $\theta(t) = \theta(t) + \delta\theta(t)$. For a component near order k, the induced phase error is approximately $k\delta\theta$(t), so the expected local peak spread satisfies $\Delta k_{peak} \approx k\ sup_t|\delta\theta(t)|/(2\pi)$ to leading order. This analytical scaling is consistent with **Table 3**: higher harmonics exhibit larger peak-order intervals because phase-warp amplification grows approximately linearly with order.

Table 3. Peak-order interval and local band power bounds.

Target order	Peak (nom)	Peak min	Peak max	Local band power (nom)	min	max	Rel. band width
1×	1.0107	1.0107	1.0107	2.0094	2.0081	2.0084	1.05×10^{-4}
2×	2.0215	1.9775	2.0215	0.3887	0.3888	0.3889	1.62×10^{-4}
5×	5.0098	4.9658	5.0537	0.2039	0.2029	0.2032	1.37×10^{-3}

Figure 3 provides a complementary time-order view of this behavior. The brightest hot zones are concentrated near the dominant order ridges and become more pronounced during the faster portion of the run-up, where small bounded errors in angular speed accumulate into larger local phase deviations. The pattern is therefore not spatially uniform: low-order content remains comparatively compact, whereas higher-order ridges show broader uncertainty halos because the same phase perturbation is multiplied by a larger harmonic index.

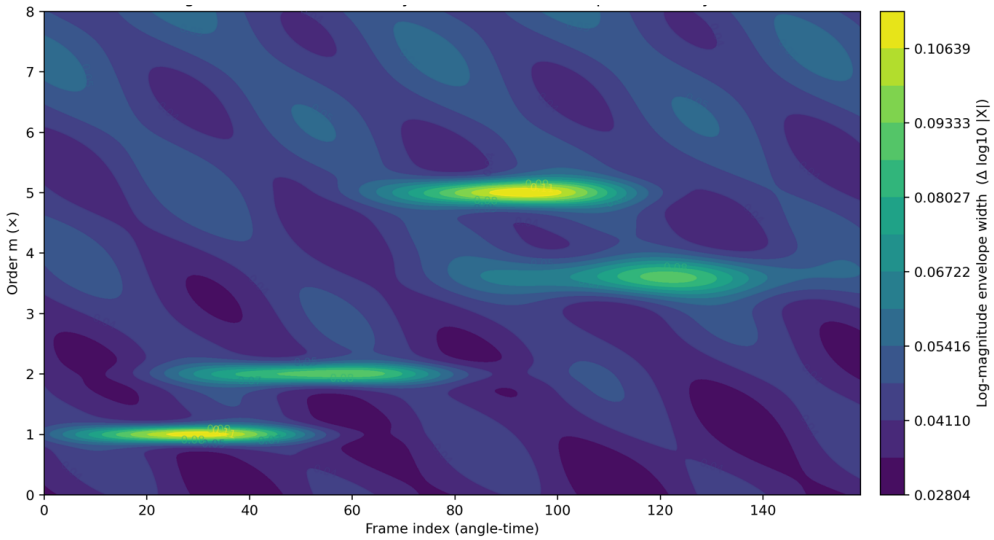

Figure 3. Interval uncertainty width in the order map.

5.3. Coverage-width trade-off under uncertainty scaling

To show how interval uncertainty impacts envelopes, we scale the speed bounds by $s \in \{0.5, 1, 1.5, 2, 3\}$ and compute coverage Equation (27) and width (28) over $0.1 - 8\times$.

Figure 4 quantifies how increasing bounded uncertainty in the speed/phase model affects the quality of the interval order-PSD envelope.

The uncertainty set is scaled by a factor s so that $\omega(t) \in [\omega_s^-(t), \omega_s^+(t)]$ widens with s, producing a broader family of admissible resampling maps $t_s(\theta)$ and therefore a broader spectral envelope $[S_s^-(m), S_s^+(m)]$. The average relative envelope width summarizes conservatism, for example

$$\mathrm{Wid}(s) = \frac{1}{|\mathcal{B}|} \sum_{m_i \in \mathcal{B}} \frac{S_s^+(m_i) - S_s^-(m_i)}{S_{ref}(m_i) + \varepsilon},$$

computed over an order band $\mathcal{B}$. The coverage fraction measures inclusion of a

reference/nominal spectrum (or surrogate truth) within the envelope:

$$\mathrm{Cov}(s) = \frac{1}{|\mathcal{B}|} \sum_{m_i \in \mathcal{B}} \mathbf{1}\left(S_{ref}\left(m_i\right) \in \left[S_s^-\left(m_i\right), S_s^+\left(m_i\right)\right]\right).$$

As s increases, envelope width grows, reflecting stronger mapping/resampling uncertainty. However, coverage may decrease when the envelope is constructed only from endpoint mappings (lower/upper speed bounds): for some order bins, the true worst-case spectrum can be attained by an interior admissible mapping rather than the endpoints.

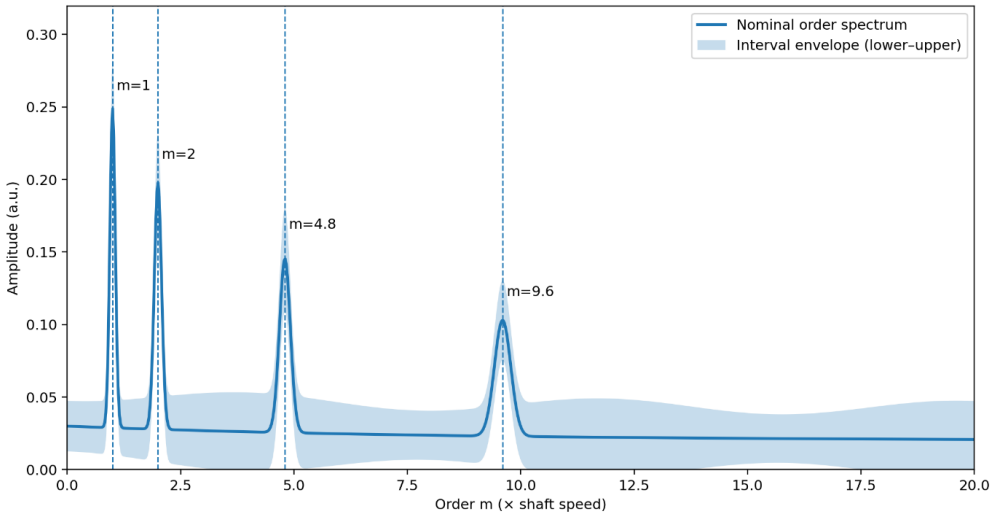

Figure 4. Coverage-width trade-off under uncertainty scaling.

A fast enclosure can be obtained by evaluating only the endpoint maps θ^- and θ^+ and taking the pointwise min-max of the resulting spectra. This endpoint-only envelope is efficient, but when the uncertainty set becomes large, it may fail to enclose $S_{\text{true}}\left(m\right)$ at every order bin because the mappinginduced spectral distortion is not necessarily monotone with respect to the uncertain resampling map. In such cases, coverage can be improved by enriching the admissible set in two standard ways: (i) multimap sampling, where additional admissible trajectories $\omega^{(j)}(t) \in [\omega^-(t), \omega^+(t)]$ are generated and the envelope is taken across j; and (ii) optimization-based bounding, where for each order m one solves a constrained min/max problem for the PSD over the admissible set, yielding tighter but more expensive bounds. These are classical set-membership tightening strategies in non-probabilistic UQ.

From a diagnostic standpoint, the acceptable balance between coverage and width depends on the use case. For screening indicators, a somewhat wider envelope may be acceptable if it preserves high inclusion of plausible spectra; for threshold-based alarms, excessively wide intervals can reduce actionability even when coverage is high. A practical rule is to prefer the cheapest envelope that keeps the local band metric stable and the coverage fraction above a user-defined target over the order band of interest. When coverage drops while width grows, as in **Table 4**, the issue is usually not insufficient conservatism in principle but under-resolution of the admissible map set by the endpoint method.

Table 4. Coverage and envelope-width metrics with respect to the uncertainty scale factor.

Uncertainty scale s	Avg. relative width ($0.1-8\times$)	Coverage fraction
0.5	0.3549	0.6611
1.0	0.9080	0.5611
1.5	2.4945	0.5556
2.0	7.2297	0.5222
3.0	27.2517	0.3944

6. Discussion

6.1. What the numerical results show about interval propagation

The numerical experiment shows that bounded uncertainty in the speed/phase model propagates into the order domain through two coupled but distinguishable effects: (i) peakorder localization uncertainty and (ii) amplitude/energy uncertainty in the order-PSD. Let the admissible resampling maps be generated by $\omega(t) \in [\omega^-(t), \omega^+(t)]$, yielding a family of angle mappings $\theta(t)$ and inverse maps $t(\theta)$. For each admissible mapping, an order-PSD $S^{(j)}(m)$ is computed; the interval envelope is then

$$S^-(m) = \min_j S^{(j)}(m),\ S^+(m) = \max_j S^{(j)}(m),$$

and the nominal spectrum $\bar{S}(m)$ is obtained from the nominal mapping (e.g., $\omega(t)$ or $\widehat{\theta}(t)$).

Peak localization: For a target order component, define the peak order as $m_p^{(j)} = \arg\max_{m\in \mathrm{N}} S^{(j)}(m)$ over a small neighborhood N around the nominal peak. The peak-order interval reported in **Table 3** can be summarized by

$$\Delta m_p = m_p^{\max} - m_p^{\min}.$$

Table 3 shows that the $1\times$ component is essentially invariant under the admissible mappings: $m_p^{\min} = m_p^{\max} = 1.0107$, hence $\Delta m_p = 0$. In contrast, the $2\times$ component exhibits $\Delta m_p = 2.0215 - 1.9775 = 0.0440$, and the $5\times$ component exhibits a larger spread $\Delta m_p = 5.0537 - 4.9658 = 0.0879$. This monotone increase of peak-order spread with order is consistent with the sensitivity of harmonics to phase warping: for a component $x(\theta) = A\cos(m_0\theta)$, a mapping perturbation $\theta \mapsto \theta + \delta\theta(\theta)$ produces a phase perturbation $m_0\delta\theta(\theta)$, so the effective distortion (and hence leakage/peak shift) scales with m_0.

Amplitude/energy robustness: For diagnostics, a more stable quantity than a single-bin peak height is the local band power around each order, defined for a narrow band $[m_1, m_2] \subset \mathrm{N}$ by

$$W_{\text{band}} = \int_{m_1}^{m_2} S(m)dm,\ W_{\text{band}}^{\pm} = \int_{m_1}^{m_2} S^{\pm}(m)dm.$$

Table 3 indicates that these interval bounds remain tight even when peak order shifts are nonzero. The reported relative widths (last column) are small for the dominant components (e.g., 1.05×10^{-4} for $1\times$ and 1.62×10^{-4} for $2\times$), and

remain modest even for $5 \times \left(1.37 \times 10^{-3}\right)$. Practically, this means that in this case study the admissible resampling maps redistribute energy slightly across nearby bins, but the integrated energy in a narrow neighborhood remains stable. Therefore, uncertainty-aware health indicators built on $W^{\pm}_{\text{band}}$ are expected to be more robust than indicators based solely on a single-bin maximum.

6.2. Interpreting the uncertainty "hot spots" in the order map

Figure 3 complements **Table 3** by revealing where (in angle-time) mapping uncertainty amplifies spectral uncertainty. Let $\left|X^{(j)}(m,k)\right|$ denote the magnitude of an order-map (time-order) representation at order m and frame index k. From the admissible set, define pointwise magnitude bounds

$$|X|^{-}(m,k) = \min_{j} \left|X^{(j)}(m,k)\right|, \; |X|^{+}(m,k) = \max_{j} \left|X^{(j)}(m,k)\right|.$$

A numerically stable way to visualize inflation is the log-magnitude envelope width

$$\Delta(m,k) = \log_{10}\left(|X|^{+}(m,k)\right) - \log_{10}\left(|X|^{-}(m,k)\right),$$

which is precisely the quantity represented by the "brightness" in **Figure 3**. Large $\Delta(m,k)$ indicates that admissible variations in $t(\theta)$ (equivalently, in $\theta(t)$) induce significant local variation in amplitude concentration at that order and frame.

To interpret hot spots quantitatively, one can define summary statistics over an order band B and/or a time window K. Two useful aggregates are:

$$\Delta_{\text{time}}(k) = \frac{1}{|\mathrm{B}|} \sum_{m_i \in \mathrm{B}} \Delta(m_i,k), \; \Delta_{\text{order}}(m) = \text{ quantile }_{k \in \mathrm{K}} \{\Delta(m,k)\} \; (e.g., 95\%).$$

In this study, the visually prominent hot regions in **Figure 3** occur in the vicinity of the dominant orders and during portions of the run-up where the local phase progression is most difficult to estimate. This behavior is expected: when acceleration increases, small speed-estimation errors accumulate into larger deviations in $\theta(t)$, widening the admissible inverse maps $t(\theta)$, and therefore widening the envelope $|X|^{\pm}(m,k)$.

6.3. Coverage-width trade-off and what it implies for envelope construction

The main quantitative validation of the interval envelope construction is captured by the coverage-width trade-off in **Figure 4** and **Table 4**, evaluated over the $0.1 - 8\times$ band. As the uncertainty scale s increases, the average relative envelope width grows rapidly (from ≈ 0.35 at $s = 0.5$ to ≈ 27 at $s = 3$), which is expected because the mapping interval $[\theta^{-}, \theta^{+}]$ widens under larger $[\omega^{-}, \omega^{+}]$. However, the observed coverage fraction decreases with increasing s. This behavior is important to interpret correctly.

In the current implementation, the envelope was computed using the two endpoint mappings (lower/upper) and taking pointwise min/max bounds in the PSD domain. While this is computationally efficient, it is not guaranteed to be a mathematically tight enclosure for all bins when the mapping-induced distortion is non-monotone

with respect to the uncertain speed function. In other words, for some order bins, the worst-case spectrum may arise from an interior admissible mapping rather than from the endpoints. When uncertainty becomes large, this phenomenon becomes more likely, leading to reduced coverage even as envelope width increases. This is precisely what **Table 4** indicates: increased uncertainty does not automatically translate into better inclusion when the bound construction is under-parameterized.

This motivates a clear methodological implication for the paper: when s is moderate to large (or when acceleration and multi-component interference are strong), the envelope construction should incorporate either (i) a small number of intermediate admissible mappings (multi-map sampling inside the interval set) or (ii) a tighter set-membership bound construction that better approximates the true supremum/infimum across admissible $\omega(t)$.

6.4. Uncertainty-aware decision metrics derived from interval spectra (replacement text)

A key benefit of the proposed interval-valued order spectrum is that it supports decision-making with bounded confidence rather than point estimates. Let the order-PSD be enclosed by the propagated interval envelope

Practitioners should interpret a wide envelope neither as an automatic fault declaration nor as a failure of the method. Rather, it indicates that the diagnostic conclusion is sensitive to admissible mapping uncertainty in that order band. If the envelope widens around a known fault order while the band-integrated energy still remains decisively above threshold, the diagnosis can remain robust; if both the envelope and the decision interval widen substantially, then the appropriate conclusion is that additional speed information or a tighter uncertainty model is needed before making a confident maintenance decision.

$$S(m) \in \left[S^{-}(m), S^{+}(m)\right],\ m \in \mathrm{B},$$

over an evaluation band $B \subset R^{+}$. A practical health indicator is the band-integrated order energy over an order interval $[m_1, m_2] \subset \mathbf{B}$,

$$W_{\text{band}} = \int_{m_1}^{m_2} S(m)dm.$$

Since integration is monotone, the interval spectrum immediately yields deterministic bounds

$$W_{\text{band}}^{-} = \int_{m_1}^{m_2} S^{-}(m)dm,\ W_{\text{band}}^{+} = \int_{m_1}^{m_2} S^{+}(m)dm,$$

so that $W_{\text{band}} \in \left[W_{\text{band}}^{-}, W_{\text{band}}^{+}\right]$. These bounds directly propagate mapping/ resampling uncertainty to a scalar metric used in maintenance decisions. When a level representation is preferred, the corresponding bounded band level is

$$L_{W,\,\text{band}}^{-} = 10\log_{10}\left(\frac{W_{\text{band}}^{-}}{W_{\text{ref}}}\right),\ L_{W,\,\text{band}}^{+} = 10\log_{10}\left(\frac{W_{\text{band}}^{+}}{W_{\text{ref}}}\right),$$

where W_{ref} is a fixed reference. In this study, **Table 3** illustrates that while peak locations may shift under admissible mappings (e.g., nonzero Δm_p for $2\times$ and $5\times$), the corresponding local energy bounds remain comparatively tight, implying that W_{band} is a robust decision feature even when single-bin maxima are sensitive to resampling.

To connect the interval metric to a decision rule, define a diagnostic statistic $D = g(W_{\text{band}})$ and a threshold τ. For monotone $g(\cdot)$ (including $g(x) = x$ or $g(x) = 10\log_{10}(x/W_{\text{ref}})$), the admissible range of D is

$$D \in \left[D^-, D^+\right] = \left[g\left(W_{\text{band}}^-\right), g\left(W_{\text{band}}^+\right)\right].$$

A conservative, uncertainty-aware exceedance statement can then be made without assuming a probability model:

$$\text{certain exceedance if } D^- > \tau, \quad \text{certain non-exceedance if } D^+ \leq \tau.$$

Only when $\tau \in (D^-, D^+)$ does the decision become ambiguous, indicating that either the uncertainty bounds should be tightened (e.g., improved speed estimation) or more data should be acquired. If a probabilistic summary is desired, the interval-valued statistic naturally induces bounds on exceedance probability under an assumed stochastic model for the remaining aleatory variability:

$$P(D > \tau) \in \left[P^-(\tau), P^+(\tau)\right],$$

where P^- and P^+ are computed by combining the deterministic interval bounds $[D^-, D^+]$ with the adopted distributional model for residual variability (e.g., segment-to-segment variability under Welch averaging). Thus, the proposed framework supports both (i) purely set-based robust decisions and (ii) probability-of-exceedance reporting, while keeping the effect of mapping uncertainty explicit and measurable through $[S^-, S^+]$ and $[W_{\text{band}}^-, W_{\text{band}}^+]$.

7. Conclusion

7.1. Main findings

This paper presented an uncertainty-aware order-tracking approach that reports an interval order spectrum instead of a single curve when the uncertainty in the speed/angle estimate is modeled as a bounded interval. By assuming, the resampling map becomes uncertain, and the order-PSD is enclosed as

$$S(m) \in \left[S^-(m), S^+(m)\right].$$

This provides a direct and interpretable measure of confidence in the order spectrum under tacholess or imperfect speed estimation.

7.2. What the results indicate

The numerical study shows that bounded mapping uncertainty produces small but visible peak-location intervals for higher harmonics (e.g., $2\times$ and $5\times$), while the

corresponding local band-energy bounds can remain tight when the tonal content is strong and well separated. The order-map uncertainty visualization highlights that uncertainty is not uniform in time; it concentrates in segments where the admissible mappings diverge most. The scaling study further confirms a practical trend: widening bounds increases envelope width and may reduce inclusion when only endpoint maps are used, motivating enriched enclosures when uncertainty is large.

7.3. Practical implications for vibration diagnostics

For engineering use, the method supports reporting diagnostic features as bounded quantities, for example

$$W_{\text{band}} \in \left[W_{\text{band}}^{-}, W_{\text{band}}^{+}\right], \; L_{W,\,\text{band}} \in \left[L_{W,\,\text{band}}^{-}, L_{W,\,\text{band}}^{+}\right],$$

which enables robust decisions. If a threshold τ is applied to a monotone statistic D, then $D^{-} > \tau$ implies certain exceedance and $D^{+} \leq \tau$ implies certain non-exceedance; otherwise the decision is ambiguous and requires tighter bounds or additional data.

7.4. Limitations and future work

The present implementation emphasizes computational practicality and, for large uncertainty, endpoint-only envelopes may be insufficient in some bins. Future work will focus on improved enclosure strategies (multi-map sampling or optimization-based bounds), and validation on experimental variable-speed datasets from rotating machinery to establish recommended settings for routine condition monitoring. Future work will also compare Welch envelopes with multitaper variants under the same interval maps and will validate the proposed framework on experimental variable-speed vibration datasets from rotating machinery test rigs and field measurements.

Author contributions: Conceptualization, SIM and YN; methodology, SIM, YN and MA; software, SIM; validation, SIM., YN, RV and AKS; formal analysis, SIM, YN and RV; investigation, YN, SIM and MA; resources, YN and AV; data curation, SIM; writing—original draft preparation, YN and SIM; writing—review and editing, YN, MA, RV, AV and AKS; visualization, SIM; supervision, YN; project administration, YN and AV; funding acquisition, SIM and AV. All authors have read and agreed to the published version of the manuscript.

Funding: This research was partially funded by INTI International University.

Institutional review board statement: Not applicable.

Informed consent statement: Not applicable.

Data availability statement: The datasets and scripts used in this study for the case study are available from the corresponding author upon reasonable request.

Conflict of interest: The authors declare that there is no conflict of interest.

References

1. Welch P. The use of fast Fourier transform for the estimation of power spectra: A method based on time averaging over short, modified periodograms. IEEE Transactions on Audio and Electroacoustics. 1967; 15(2): 70–73. doi: 10.1109/TAU.1967.1161901
2. Thomson DJ. Spectrum estimation and harmonic analysis. Proceedings of the IEEE. 1982; 70(9): 1055–1096. doi: 10.1109/PROC.1982.12433
3. Borghesani P, Pennacchi P, Chatterton S, et al. The velocity synchronous discrete Fourier transform for order tracking in the field of rotating machinery. Mechanical Systems and Signal Processing. 2014; 44(1–2): 118–133. doi: 10.1016/j.ymssp.2013.03.026
4. Peeters C, Leclère Q, Antoni J, et al. Review and comparison of tacholess instantaneous speed estimation methods on experimental vibration data. Mechanical Systems and Signal Processing. 2019; 129: 407–436. doi: 10.1016/j.ymssp.2019.02.031
5. Lu S, Yan R, Liu Y, et al. Tacholess Speed Estimation in Order Tracking: A Review With Application to Rotating Machine Fault Diagnosis. IEEE Transactions on Instrumentation and Measurement. 2019; 68(7): 2315–2332. doi: 10.1109/TIM.2019.2902806
6. Combet F, Gelman L. An automated methodology for performing time synchronous averaging of a gearbox signal without speed sensor. Mechanical Systems and Signal Processing. 2007; 21(6): 2590–2606. doi: 10.1016/j.ymssp.2006.12.006
7. Schmidt S, Heyns PS, De Villiers JP. A tacholess order tracking methodology based on a probabilistic approach to incorporate angular acceleration information into the maxima tracking process. Mechanical Systems and Signal Processing. 2018; 100: 630–646. doi: 10.1016/j.ymssp.2017.07.053
8. Xu L, Chatterton S, Pennacchi P, et al. A Tacholess Order Tracking Method Based on Inverse Short Time Fourier Transform and Singular Value Decomposition for Bearing Fault Diagnosis. Sensors. 2020; 20(23): 6924. doi: 10.3390/s20236924
9. Wang Y, Xu G, Luo A, et al. An online tacholess order tracking technique based on generalized demodulation for rolling bearing fault detection. Journal of Sound and Vibration. 2016; 367: 233–249. doi: 10.1016/j.jsv.2015.12.041
10. Hu Y, Tu X, Li F, et al. An adaptive and tacholess order analysis method based on enhanced empirical wavelet transform for fault detection of bearings with varying speeds. Journal of Sound and Vibration. 2017; 409: 241–255. doi: 10.1016/j.jsv.2017.08.003
11. Pan MC, Chu WC, Le DD. Adaptive angular-velocity Vold–Kalman filter order tracking—Theoretical basis, numerical implementation and parameter investigation. Mechanical Systems and Signal Processing. 2016; 81: 148–161. doi: 10.1016/j.ymssp.2016.03.013
12. Feng K, Ji JC, Wang K, et al. A novel order spectrum-based Vold-Kalman filter bandwidth selection scheme for fault diagnosis of gearbox in offshore wind turbines. Ocean Engineering. 2022; 266: 112920. doi: 10.1016/j.oceaneng.2022.112920
13. Urbanek J, Barszcz T, Antoni J. A two-step procedure for estimation of instantaneous rotational speed with large fluctuations. Mechanical Systems and Signal Processing. 2013; 38(1): 96–102. doi: 10.1016/j.ymssp.2012.05.009
14. Zhao M, Lin J, Wang X, et al. A tacho-less order tracking technique for large speed variations. Mechanical Systems and Signal Processing. 2013; 40(1): 76–90. doi: 10.1016/j.ymssp.2013.03.024
15. Abboud D, Antoni J, Sieg-Zieba S, et al. Envelope analysis of rotating machine vibrations in variable speed conditions: A comprehensive treatment. Mechanical Systems and Signal Processing. 2017; 84: 200–226. doi: 10.1016/j.ymssp.2016.06.033
16. Borghesani P, Pennacchi P, Randall RB, et al. Order tracking for discrete-random separation in variable speed conditions. Mechanical Systems and Signal Processing. 2012; 30: 1–22. doi: 10.1016/j.ymssp.2012.01.015
17. Borghesani P, Ricci R, Chatterton S, et al. A new procedure for using envelope analysis for rolling element bearing diagnostics in variable operating conditions. Mechanical Systems and Signal Processing. 2013; 38(1): 23–35. doi: 10.1016/j.ymssp.2012.09.014
18. Borghesani P, Pennacchi P, Randall RB, et al. Application of cepstrum pre-whitening for the diagnosis of bearing faults under variable speed conditions. Mechanical Systems and Signal Processing. 2013; 36(2): 370–384. doi: 10.1016/j.ymssp.2012.11.001
19. Borghesani P, Pennacchi P, Chatterton S. The relationship between kurtosis- and envelope-based indexes for the

diagnostic of rolling element bearings. Mechanical Systems and Signal Processing. 2014; 43(1–2): 25–43. doi: 10.1016/j.ymssp.2013.10.007
20. Randall RB, Antoni J, Chobsaard S. The Relationship Between Spectral Correlation and Envelope Analysis in the Diagnostics of Bearing Faults and Other Cyclostationary Machine Signals. Mechanical Systems and Signal Processing. 2001; 15(5): 945–962. doi: 10.1006/mssp.2001.1415
21. Chen B, Zhang W, Xi GJ, et al. Product envelope spectrum optimization-gram: An enhanced envelope analysis for rolling bearing fault diagnosis. Mechanical Systems and Signal Processing. 2023; 193: 110270. doi: 10.1016/j.ymssp.2023.110270
22. Wu K, Tong W, Xie J, et al. Optimal Weighted Envelope Spectrum: An enhanced demodulation method for extracting specific characteristic frequency of rotating machinery. Mechanical Systems and Signal Processing. 2024; 211: 111165. doi: 10.1016/j.ymssp.2024.111165
23. Schmidt S, Wilke DN, Gryllias KC. Generalised envelope spectrum-based signal-to-noise objectives: Formulation, optimisation and application for gear fault detection under time-varying speed conditions. Mechanical Systems and Signal Processing. 2025; 224: 111974. doi: 10.1016/j.ymssp.2024.111974
24. Kliemank ML, Rupprecht B, Ahmadzadeh M, et al. Online instantaneous angular speed estimation from vibration on low-power embedded systems evaluated on a gas foil bearing use case. Measurement: Sensors. 2025; 38: 101600. doi: 10.1016/j.measen.2024.101600
25. Behrendt M, Dang C, Beer M. Projecting interval uncertainty through the discrete Fourier transform: Application to time signals with poor precision. Mechanical Systems and Signal Processing. 2023; 177: 109192.
26. Behrendt M, Dang C, Beer M. Data-driven and physics-based interval modelling of power spectral density functions from limited data. Mechanical Systems and Signal Processing. 2024; 208: 111078. doi: 10.1016/j.ymssp.2023.111078
27. Behrendt M, De Angelis M, Beer M. Uncertainty Propagation of Missing Data Signals with the Interval Discrete Fourier Transform. ASCE-ASME Journal of Risk and Uncertainty in Engineering Systems, Part A: Civil Engineering. 2023; 9(3): 04023022. doi: 10.1061/AJRUA6.RUENG-1048
28. Liu G, Kreinovich V. Fast convolution and Fast Fourier Transform under interval and fuzzy uncertainty. Journal of Computer and System Sciences. 2010; 76(1): 63–76. doi: 10.1016/j.jcss.2009.05.006
29. Rodopoulos KI, Antoniadis IA. Instantaneous fault frequencies estimation in roller bearings via wavelet structures. Journal of Sound and Vibration. 2016; 383: 446–463. doi: 10.1016/j.jsv.2016.07.027
30. Zeng R, Zhang L, Xiao Y, et al. A Method Combining Order Tracking and Fuzzy C-Means for Diesel Engine Fault Detection and Isolation. Shock and Vibration. 2015; 2015: 1–7. doi: 10.1155/2015/547238
31. Zhang Y. Interpretable and Uncertainty-Aware Multi-Modal Spatio-Temporal Deep Learning Framework for Regional Economic Forecasting. HighTech and Innovation Journal. 2025; 6(4): 1300–1314. doi: 10.28991/HIJ-2025-06-04-010
32. Naidu IES, Padmavathi T, Padmavathi SV, et al. Intelligence Based Controlling Models for Effective Power Tracking and Voltage Enhancement in Grid-PV Systems. Emerging Science Journal. 2025; 9(1): 261–283. doi: 10.28991/ESJ-2025-09-01-015